

Photoconductivity measurements of x-ray-absorption spectra of tetramethyl tin in 2,2,4-trimethylpentane near the Sn *K* edge

T. K. Sham

Department of Chemistry, The University of Western Ontario, London, Ontario, Canada N6A 5B7

R. A. Holroyd

Chemistry Department, Brookhaven National Laboratory, Upton, New York 11973

(Received 18 August 1988; revised manuscript received 5 December 1988)

X-ray-induced photoconductivity is used to record the x-ray-absorption spectra of solutions of tetramethyl tin, $(\text{CH}_3)_4\text{Sn}$, in 2,2,4-trimethylpentane near the Sn *K* edge (29.2 keV). It is found that at low concentrations the edge jump observed in the conductivity (ionization yield) spectrum is similar to that of the normal absorption spectrum, while at higher concentrations the conductivity edge jump is inverted, an observation consistent with previous findings. It is also observed for the first time that a changeover from normal to an inverse edge jump takes place at a narrow region of concentrations. An additivity model of ionization yields is introduced. It is shown that this model can be used to explain the results and to predict the correct concentration where the inversion of the absorption edge occurs.

I. INTRODUCTION

X-ray-induced conductivity of liquid hydrocarbons and their solutions have been recently investigated with synchrotron radiation¹⁻⁵ in connection with the development of extended x-ray-absorption fine-structure (EXAFS) measurement techniques and the ionization properties of these liquids. It was found in these experiments that the ionization yield (directly derived from conductivity) of several hydrocarbon liquids in x-ray energies between 5 and 30 keV depends not only on the total energy absorbed but also on the energy of the photon.³ For example, the ionization yield induced by the absorption of a 20-keV photon is about 30% higher than that of two 10-keV photons. It was also reported that in dilute solutions of organometallics in a thin cell configuration, the x-ray-induced photocurrent generally follows the appearance of the absorption coefficient of an absorption edge while in concentrated solutions, and in a thick cell configuration the photocurrent exhibits an anomalous behavior: that is, that it actually drops above an absorption edge. This behavior is now understood qualitatively for the limiting cases of thin and thick samples.⁵ Relatively little effort, however, has been made to investigate the intermediate concentrations. As an extension of the previous work and for the completion of these studies, we report here some recent measurements of organometallics in hydrocarbons and propose an additivity model of ionization yields, with which we can now explain and predict quantitatively the behavior of the x-ray-induced photoconductivity across an absorption edge at any intermediate concentration (absorption coefficient).

Our experimental approach to the quantitative understanding of the problem is to study the ionization behavior of the solvent and the solute separately, and the concentration dependence of the conductivity near an absorption edge. The data analysis is carried out according to an additivity model of ionization. This model is based

on the absorption and ionization characteristics of the solvent and solute and is discussed in this paper in some details for the first time. The solvent and solute selected for the experiments are 2,2,4-trimethylpentane (henceforth denoted 2,2,4-TMP) and tetramethyltin, $(\text{CH}_3)_4\text{Sn}$, respectively. The ionization behavior of 2,2,4-TMP has already been documented,³ $(\text{CH}_3)_4\text{Sn}$ is a liquid and has a high-energy *K* edge (~ 29.2 keV) in Sn. At this energy, high-efficiency measurements are easily achievable. The complete study of the ionization behavior of neat $(\text{CH}_3)_4\text{Sn}$ liquid with (5–30)-keV photons will be discussed elsewhere.⁶ Here, we focus on dilute concentrations where the solute is surrounded by multiple shells of solvent molecules. The experimental methods are briefly described in Sec. II, followed by the results of photocurrent measurements of a series of $(\text{CH}_3)_4\text{Sn}$ solutions near the Sn *K* edge in Sec. III. Discussion is presented in Sec. IV and conclusions in Sec. V.

II. EXPERIMENT

X-ray-absorption measurements were carried out at the C2 station of the Cornell High Energy Synchrotron Source (CHESS) using Si(220) crystals. The liquid-cell assembly employed in the experiments has been described previously.^{2,3} It has a parallel-electrode configuration similar to that of the gas-ionization chambers. The separation between the electrodes is either 0.3 or 0.5 cm. The length of the cell is 3 cm (so are the parallel electrodes). Both configurations were used for the measurements. The cell is made of Pyrex with Mylar windows. The incoming x-ray beam is defined by a narrow horizontal slit of ~ 0.1 mm width. This arrangement produces a very thin slab of ionization region in the liquid and excellent photon-energy resolution.

The liquid cell is placed in a metal container filled with dry nitrogen during the measurements. High voltage is applied to one electrode and the current measured at the

other with a current amplifier. The incoming and transmitted flux of the monochromatic beam is monitored with two Ar ionization chambers placed in front of and behind the liquid cell,³ respectively. Current signals from all three detectors were recorded with scaler-voltage-to-frequency converter counting devices.

Data acquisition was with a VAX computer system.

From these measurements, the actual number of photons/s incident upon the solution and the number of photons/s absorbed by the solution can be calculated from the following expression,

$$I = i(\text{Ar})WF \exp[-\mu(\text{Ar})T]/eE \{1 - \exp[-\mu(\text{Ar})T]\} \text{ photon/s}, \quad (1)$$

where I and i are the incident-photon flux on the liquid sample and the current from the Ar-ion chamber (beam monitor), respectively; W is the energy required to form an ion pair (27 eV for Ar), F the fraction of the transmitted photons actually seen by the liquid after air, and window and dry gas absorption have been accounted for and is 0.991 at the Sn K edge.³ μ is the absorption coefficient, which is simply the concentration times the absorption cross section,⁷ T the length of the plates in the ion chamber, e the electron charge, and E the energy (eV) of the photon. Using I , we can calculate the ionization yield Y (in e^-/eV) with

$$Y = i(\text{liq})/IeE \{1 - \exp[-\mu(\text{liq})t]\}, \quad (2)$$

where $i(\text{liq})$ is the photocurrent in the liquid cell. The unit of Y is electronic charge per eV of photon energy absorbed. Y multiplied by 100 is the conventional G value used in radiation chemistry and Y multiplied by the photon energy is the charge produced by the absorption of a photon at the energy of interest.³⁻⁵

X-ray-absorption spectra were simultaneously recorded in the transmission and current-yield modes at a field strength of either 2 kV/cm or 5 kV/cm. These field strengths, together with the narrow entrance slit, assure a near-unity collection efficiency of free ions. The absorption spectra recorded in the current mode are displayed as current yield versus photon energy. It should be noted that the spectra are recorded with respect to the same number of incident photons (I_0), while the ionization yield is normalized to the number of photons absorbed ($I_0[1 - \exp(-\mu t)]$). Thus the $1 - \exp(-\mu t)$ factor must be taken into account for quantitative discussion of the spectrum in terms of ion yields Y .

Two series of measurements have been made under slightly different conditions. In the first series (henceforth denoted series A), we employed a cell with a 5-mm electrode separation and a 2-(kV/cm) field strength, and chose, somewhat arbitrarily, dilute and concentrated solutions that would yield normal and inverse Sn K -edge spectrum in the conductivity mode. In the second series (henceforth denoted series B), we used a cell with a 3-mm separation and a 5-(kV/cm) field strength, and used samples that were prepared within a narrow region of concentrations of which the edge jump in the conductivity Sn K -edge spectrum is expected to change from up to down according to the additivity model of ionization yields.

III. RESULTS

The absorption and current yield spectra of series A and B are shown in Figs. 1 and 2 respectively. It is apparent from Fig. 1 that at low concentrations the current-yield spectrum resembles the absorption, while at high concentrations the current-yield spectrum turns upside down at the edge. In Fig. 2 we can see that at the concentration of 0.074 M, the spectrum begins to lose its near-edge resonance features and at 0.092 M it develops an unusual shape (partly going up and partly going down) and bears no resemblance to the absorption spectrum. This observation indicates that an inversion is already underway. As the concentration increases further to 0.105 M, the spectrum is completely inverted. The concentrations of the solutions and the results are summarized in Table I together with other relevant parameters such as the absorption μt (where μ is the absorption cross section⁷ and t the cell thickness), the fractional coefficient of Sn, $\mu(\text{Sn})/\mu(\text{tot})$, and the ionization yield Y in units of e^- charge per eV photon energy absorbed at photon energies below (29.1 keV) and above (29.2 keV) the Sn K edge. The Y values for neat 2,2,4-TMP are 2.85×10^{-3} and $2.23 \times 10^{-3} e^-/\text{eV}$ at field strengths of 5 and 2 kV/cm, respectively (exact conditions under which our solution experiments were performed). The ionization yields of neat $(\text{CH}_3)_4\text{Sn}$ recorded as a function of field strengths are shown in Fig. 3, from which we can see that the yield at below (29.1 keV) and above (29.2 keV) the Sn K edge at 5 kV/cm, for example, are 2.8×10^{-3} and $1.1 \times 10^{-3} e^-/\text{eV}$, respectively.^{3,6}

IV. DISCUSSION

We first discuss the ionization yields of the neat solvent and the neat solute. We can see from the value given above that they are very similar, except that the Sn yield decreases above the K edge. This decrease in yield can be attributed to the x-ray fluorescence, part of which escapes detection.^{4,5} The field-strength dependence is similar to that of the pure solvent, as expected.^{3,4,6} It should be noted, however, that in neat $(\text{CH}_3)_4\text{Sn}$ the molecule is surrounded by the bulk of the same molecules, while in dilute solution it is surrounded by the bulk of solvent molecules. Although the chemical dependence of the electron mean free path in liquids is not well known, judging from the universal behavior of electron-energy-loss processes in solids, and previous experience with hydrocarbons,³ it is reasonable to expect that Y_{Sn} in neat

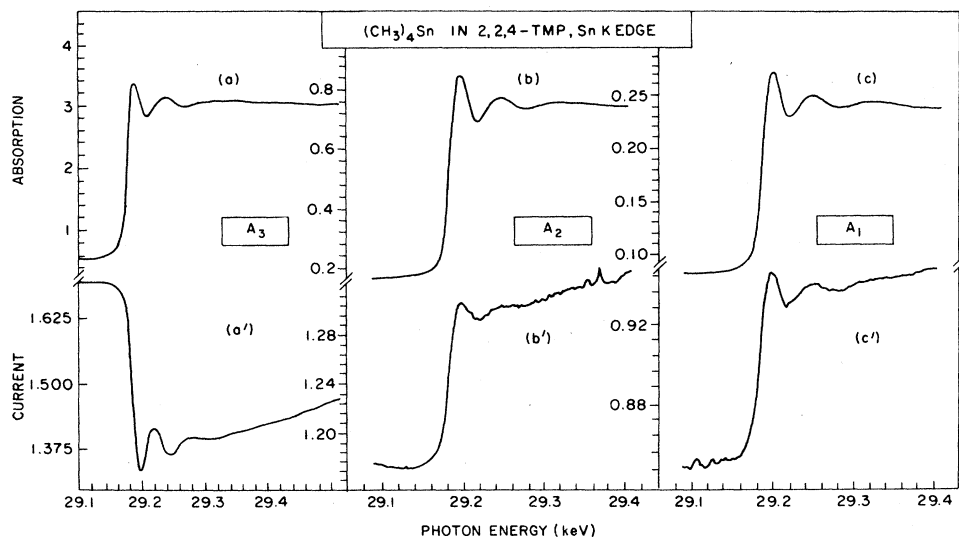


FIG. 1. Sn *K*-edge absorption and conductivity spectra of series *A*: (a)–(c), transmission spectra; (a')–(c'), conductivity spectra for solutions *A*₃, *A*₂, and *A*₁, respectively.

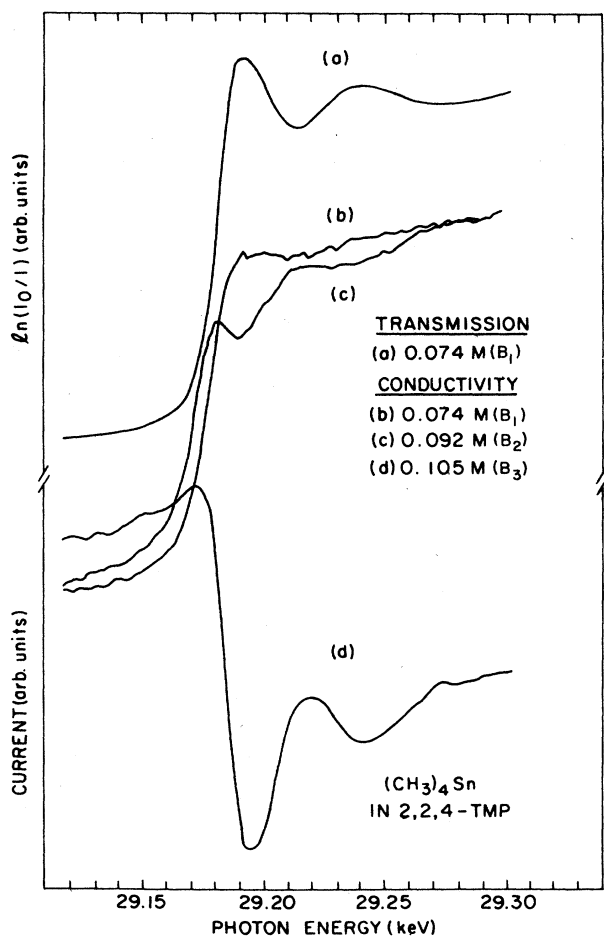


FIG. 2. Sn *K*-edge absorption and conductivity spectra of series *B*: (a), transmission spectrum of solution *B*₁; (b)–(d), conductivity spectra of solutions *B*₁–*B*₃, respectively.

liquid and in 2,2,4-TMP solution are similar (Table I and Fig. 3).⁶ Here we are primarily concerned with dilute solutions at the experimental field strengths of 2–5 kV/cm.

We next describe the physical basis of a model with which the spectra (Figs. 1 and 2) can be understood on a quantitative basis. The essence of this model lies in the notion of additivity. When the ionization properties of the solvent and solute are known, we can argue that in a solution the total ionization yield is simply a combined contribution of the solvent itself plus the contribution from the solute. In situations where the amount of solute is much less than that of the solvent (a situation encountered in the experiments reported here), only the ionization properties of the solvent are important, and the contribution of the solute to the total ionization depends almost entirely on the absorption coefficient of the solute which absorbs the photon and redistributes the energy to the solvent via photoelectron and decay processes (x-ray fluorescence and Auger decay) which further ionize the medium. The solvent molecules surrounding the solute would serve as a medium that provides secondary charges. For example, in the photoconductivity measurements of $(\text{CH}_3)_4\text{Sn}$ in 2,2,4-TMP near the Sn *K* edge, the total ionization yield arises by the absorption of ~ 29 -keV photons by the solvent and the solute. The solvent absorption creates photoelectrons with energies of 28.7 keV or higher (C *K* edge and valence band) and has a smooth ionization yield at photon energies across the Sn *K* edge. These energetic photoelectrons, which will travel a long distance (~ 0.023 mm) before they lose most of their energy and become thermalized,³ can generate a large number of secondary charges which are detected by the liquid cell as current. The Sn *K*-edge absorption cross section and the nature of the decay processes change markedly however from below to above the edge. Below the

TABLE I. Relevant parameters for conductivity measurements of solutions of $(\text{CH}_3)_4\text{Sn}$ in 2,2,4-TMP at photon energies of 29.1 and 29.2 keV.

Sample	Concentration		$h\nu=29.1$ keV (below the edge)				$h\nu=29.2$ keV (above the edge)			
	$(\text{CH}_3)_4\text{Sn}$ (M)	Sn (mg/ml)	$1-e^{-\mu t}$	Y^b ($10^{-3} e^-/eV$)	f_{Sn}	Y_{Sn}^b ($10^{-3} e^-/eV$)	$1-e^{-\mu t}$	Y^a ($10^{-3} e^-/eV$)	f_{Sn}	Y_{Sn}^a ($10^{-3} e^-/eV$)
A_1	0.0126	1.49	0.127	2.33	0.224	2.68	0.256	1.25	0.652	0.727
A_2	0.0425	5.04	0.188	2.07	0.494	1.91	0.531	0.798	0.864	0.573
A_3	0.181	21.4	0.421	1.71	0.804	1.58	0.944	0.593	0.964	0.532
B_1	0.074	8.78	0.248	2.23	0.629	2.23	0.711	0.826	0.917	0.699
B_2	0.092	10.9	0.280	2.15	0.678	2.11	0.780	0.786	0.931	0.679
B_3	0.105	12.5	0.303	2.28	0.707	2.30	0.822	0.822	0.939	0.731

threshold, the absorption cross section is only a small fraction (16%) of that above the edge, but the photoelectrons resulting from valence-band, shallow-core, and L -edge photoionization are still quite energetic. These electrons can again generate a large number of secondary charges in the surrounding solvent. At energies above the Sn K edge, on the other hand, although the absorption cross section is greater (primarily due to the ionization of the Sn $1s$ shell) and the Auger (KLL) electrons (which account for about 14% of the $1s$ hole-decay processes) are energetic, the primary photoelectrons have very low energies and the newly created x-ray-fluorescence channel has a large probability of escaping detection.^{4,5}

It can be summarized from the above discussions that there are several counteracting factors that determine the final shape of the photoconductivity spectrum across an absorption edge: First, the relative absorption between the solvent and the solute; second, the relative absorption below and above the edge; third, the ionization yield of the solvent and that of the solute in the solution; and, finally, the relative importance of the x-ray-fluorescence versus Auger decay above the edge. It is a subtle balance of these factors that leads to the observed shape of the conductivity spectrum.

The proposed model takes into account all the

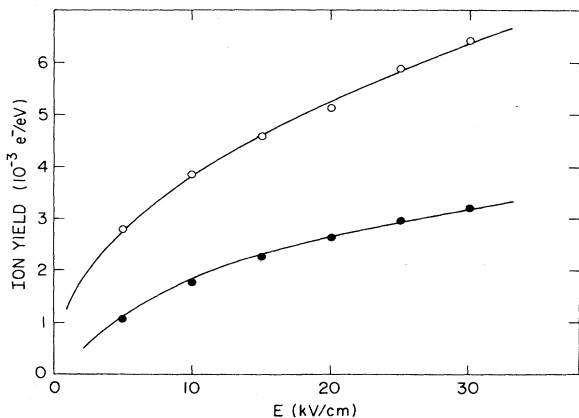


FIG. 3. Ionization yield of neat $(\text{CH}_3)_4\text{Sn}$ liquid as a function of field strength at energies below (29.1 keV), \circ , and above (29.2 keV), \bullet , the edge; the electrode separation is 1 mm.

forementioned factors with the following assumptions. First, the solution is dilute (~ 0.1 M, for example⁸); second, the total ionization yield Y_{tot} is the sum of the fractional contribution of the solvent and the solute; third, the ionization yield of the neat solvent Y_C , and that due to the solute surrounded by solvent Y_{Sn} , are assumed to be fairly constant within a narrow region of concentrations and only slowly varying among all concentrations of concern at constant photon energy. Based on these assumptions, we can derive Y_{Sn} in 2,2,4-TMP from the total yield (Table I) using the expression

$$Y_{\text{tot}} = f_C Y_C + f_{\text{Sn}} Y_{\text{Sn}}, \quad (3a)$$

where Y_{tot} is the total ionization yield of the solution and f_C and f_{Sn} ($f_C + f_{\text{Sn}} = 1$) are the fractional absorption by the solvent and the solute, respectively. Both the solvent and the solute are competing for the same photon flux; therefore

$$f_C = \mu(C) / [\mu(\text{Sn}) + \mu(C)], \quad (3b)$$

$$f_{\text{Sn}} = \mu(\text{Sn}) / [\mu(\text{Sn}) + \mu(C)], \quad (3c)$$

where $\mu(C)$ and $\mu(\text{Sn})$ are the absorption coefficients of the hydrocarbon and Sn, respectively. Since μ is equal to the product of the cross section⁷ and the concentration, these equations have already taken into account the concentrations explicitly.

Since the current depends on the product of the number of photons absorbed times Y [see Eq. (2)], the ratio of the ionization current above and below the edge, R , is

$$R = \frac{1 - e^{-\mu_a t}}{1 - e^{-\mu_b t}} \left[\frac{f_{\text{Sn}}^a Y_{\text{Sn}}^a + f_C^a Y_C^a}{f_{\text{Sn}}^b Y_{\text{Sn}}^b + f_C^b Y_C^b} \right], \quad (4)$$

where sub(super)scripts b and a denote parameters below and above the edge, respectively. The f terms can be obtained using Eqs. (3) together with tabulated cross sections.⁷ The μ terms in Eqs. (3b) and (3c) are simply the product of the mass absorption coefficient and concentration. For example, $\mu_a = \sigma_{\text{Sn}}^a [\text{Sn}] + \sigma_C^a [C]$ and $\mu_b = \sigma_{\text{Sn}}^b [\text{Sn}] + \sigma_C^b [C]$ (σ denotes mass absorption coefficient in cm^2/g and $[]$ denotes concentration in g/ml). The $[1 - \exp(-\mu t)]$ terms take into account the difference in absorption above and below the edge. Using a Y_C value of $2.23 \times 10^{-3} e^-/eV$, and Y_{Sn} values of 2.03×10^{-3} and $0.66 \times 10^{-3} e^-/eV$ (both series- A aver-

ages) for below (29.1 keV) and above (29.2 keV) the edge, respectively, and $t=3$ cm, $\sigma_{\text{Sn}}^a=43.18$, $\sigma_{\text{Sn}}^b=6.816$, $\sigma_{\text{C}}^a=0.05890$, and $\sigma_{\text{C}}^b=0.06034$, we have calculated the $(\text{CH}_3)_4\text{Sn}$ concentration dependence of R according to Eq. (4). The results are shown in Fig. 4.

Several interesting features are immediately apparent from Fig. 4. First, the ratio R increases as the concentration increases, until it reaches a maximum; then R begins to decrease. Second, at ~ 2 M, the R value already reaches the high-concentration limit and remains unchanged for further concentration increases. Finally, perhaps the most interesting feature is seen in R becoming less than unity at concentrations > 0.096 M. The first two features are expected since the increase in absorption cross section in Sn across the K edge is more important than the corresponding decrease in ion yield Y_{Sn} . The last feature has very important implications: it indicates that the edge jump becomes inverted at concentrations greater than 0.096 M. It should be noted that the R ratio for the neat 2,2,4-TMP is less than unity, because the calculation was performed at energies of 29.1 and 29.2 keV for below- and above-edge absorption, respectively, and the absorption cross section for carbon at 29.2 keV is slightly less than that at 29.1 keV.

The observed ionization yield Y of the two series of solutions are given in Table I together with the Y_{Sn} values [derived from Eqs. (3)] at selected photon energies below (29.1 keV) and above (29.2 keV) the edge. The in-

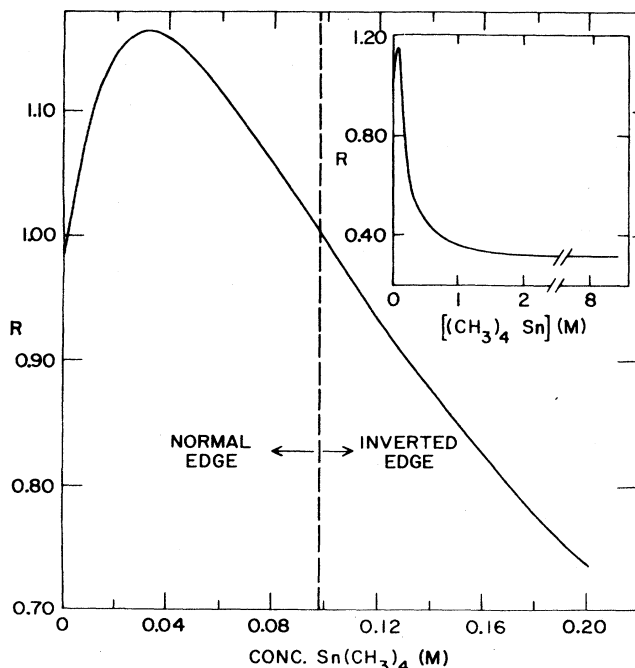


FIG. 4. Calculated ratio R of current above and below the Sn K edge of $(\text{CH}_3)_4\text{Sn}$ in 2,2,4-TMP solutions as a function of $(\text{CH}_3)_4\text{Sn}$ concentrations [Eq. (4), see text]. Insert shows R vs $[(\text{CH}_3)_4\text{Sn}]$ for the entire range of concentrations. Normal and inverted edge jump are expected to occur at concentrations lower and higher, respectively, than the concentration of $[(\text{CH}_3)_4\text{Sn}]$ at $R=1$ (the vertical line).

dividual Y_{Sn} yields from our measurements are also plotted in Fig. 5 for comparison. It can be seen from Table I that, below the edge, Y_{tot} decreases slightly with increasing Sn concentration, as expected from Eqs. (3). It can also be seen that Y_{Sn} values are fairly constant across the concentrations at fixed photon energies, except for A_1 at 29.1 keV (the origin of this deviation is not clear at present), and Y_{Sn} values are considerably smaller at energies above the edge, resulting in a significant drop in Y_{tot} . This observation is in qualitative accord with the high probability ($\sim 86\%$) of the x-ray-fluorescence decay above the K edge. These results are as expected, and hence lend support to the validity of the additivity model.

We now focus on the series-B data, which were designed according to the additivity model for the observation of the edge-jump inversion in the conductivity spectrum. We can estimate the concentration at inversion from Fig. 4, which suggests that, when the concentration is about 0.1 M, inversion or anomalous behavior in Y_{tot} at the edge (under similar experimental conditions employed in this study) should be observable in the conductivity spectrum. The concentrations used in the series-B experiments were, in fact, chosen to be in the vicinity of 0.1 M. We can see from Fig. 2 that the shape of the conductivity spectrum at these concentrations indeed undergoes a progressive changeover from a normal edge jump to a fully inverted appearance. This observation thus confirms the validity of the additivity model. Another illustration of the successful application of the model can be found in the comparison of the observed edge jump in the conductivity spectrum with those of calculation [Eq. (4)]. The results are shown in Table II. We can immediately see that the agreement is again very satisfactory.

V. CONCLUSIONS

We have presented the absorption data of $(\text{CH}_3)_4\text{Sn}$ in 2,2,4-TMP at the Sn K edge using conductivity measure-

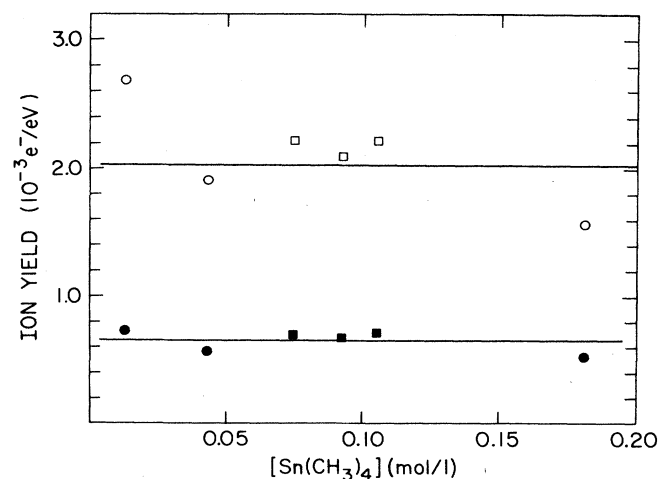


FIG. 5. Ionization yields of Sn (Y_{Sn}) below (open symbols) and above (solid symbols) the K edge at different concentrations. Circles and squares designate field strengths of 2 and 5 kV/cm, respectively.

TABLE II. Observed and predicted edge jump (%) (\uparrow and \downarrow denote normal and inverse edge jump, respectively; inversion of the peaks is visible in the spectrum of B_2) in the conductivity spectrum between 29.1 and 29.2 keV.

Sample	A_1	A_2	A_3	B_1	B_2	B_3
Observed	8.9 \uparrow	11.0 \uparrow	20 \downarrow	7.5 \uparrow	4.5 \uparrow	4.1 \downarrow
Predicted	10.7 \uparrow	15.4 \uparrow	22 \downarrow	7.5 \uparrow	2.0 \uparrow	2.1 \downarrow

ments, and explained the results in terms of an additivity model of ionization. We have also shown, with examples, how this model can be used to predict the right concentrations at which inversion at the Sn K edge can be observed. This model can be extended to concentrated solutions [this requires the knowledge of the ionization yield of neat $(\text{CH}_3)_4\text{Sn}$ in this case],⁶ and to other EXAFS measurement techniques. Finally, it should be noted that results discussed here represent a situation where sudden changes in the energy conversion and redistribution take place in an extremely small photon-energy change across an edge. This behavior may find applications in the design of liquid-state ionization detectors for x rays which could be used for edge-jump measurements at low solute concentrations.

ACKNOWLEDGMENTS

We are grateful to the staff of the Cornell High Energy Synchrotron Source (CHESS) for assistance and the use of their facility, which is supported by the U.S. National Science Foundation. Research carried out at Brookhaven National Laboratory was done so under Contract No. DE-AC02-76CH00016 with the U.S. Department of Energy and supported by its Division of Chemical Sciences, Office of Basic Energy Sciences. Research carried out at the University of Western Ontario was supported by the Ontario Centre for Materials Research (OCMR).

¹T. K. Sham and S. M. Heald, *J. Am. Chem. Soc.* **105**, 5142 (1983).

²T. K. Sham and R. A. Holroyd, *J. Chem. Phys.* **80**, 1026 (1984).

³R. A. Holroyd and T. K. Sham, *J. Phys. Chem.* **89**, 2909 (1985).

⁴T. K. Sham, R. A. Holroyd, and R. C. Munoz, *Nucl. Instrum. Methods A* **249**, 530 (1986); *J. Phys. (Paris) Colloq.* **47**, C8-1097 (1986).

⁵T. K. Sham, in *X-ray Absorption Studies of Liquids: Structure and Reactivity of Metal Complexes in Solution and X-ray Photoconductivity of Hydrocarbon Solutions of Organometallics*, Vol. 145 of *Topics in Current Chemistry*, edited by E. Mandel-

kow (Springer-Verlag, Berlin, 1988), p. 81.

⁶R. A. Holroyd and T. K. Sham (unpublished results).

⁷W. H. McMaster, N. Kerr Del Grande, J. H. Mallett, and J. H. Hubbell, *Compilation of X-Ray Cross Sections* (National Technical Information Service, Springfield, VA, 1969).

⁸At 0.1 M, each $(\text{CH}_3)_4\text{Sn}$ is surrounded by ~ 80 solvent molecules.

⁹Strictly speaking, we only consider the absorption of Sn in $(\text{CH}_3)_4\text{Sn}$; the absorption of the methyl groups is included in the carbon calculation in which the contribution of hydrogen has been neglected.